Available online at www.sciencedirect.com
SCIENCE DIRECT
Catalysis Today 104 (2005) 168–176
CATALYSIS TODAY
www.elsevier.com/locate/cattod

Influence of the operating conditions on yield and selectivity for the partial oxidation of ethane in a catalytic membrane reactor

Katya Georgieva, Ivan Mednev, Dietrich Handtke, Jürgen Schmidt *

Institute of Fluid Dynamics and Thermodynamics, Otto-von-Guericke-University Magdeburg, P.O.B. 4120, Magdeburg D-39016, Germany

Available online 12 May 2005

Abstract

In this study, simulation results are presented for the partial oxidation of ethane to ethylene in a Catalytic Membrane Reactor (CMR) under isothermal and non-isothermal conditions. Considering the importance of the transport processes, a 2D model was developed and implemented in FLUENT® using self-designed program modules for reaction kinetics, transport properties and post-processing. An analysis of significance of the influencing variables is carried out on the basis of a reference case. The number of parameters were minimized by the dimensionless formulation of the model. One of the most important variables is the oxygen dosage through the membrane. Both velocity and oxygen concentration of the trans-membrane stream were varied with the aim of attaining maximum ethylene yield. The results of the different simulations clearly show the advantages of the CMR compared to the Catalytic Wall Reactor (CWR). The numerical simulations are essential in order to reduce the experimental costs and to evaluate different reactor concepts.

Keywords: CMR; Catalytic Wall Reactor; Numerical simulation; Trans-membrane stream

1. Introduction

Membrane reactors are of increasing industrial interest, which is shown by the recent intensive research work in this area. This concerns on the one hand the development of special catalysts with high selectivity and on the other hand the process optimization for a given catalyst. An overview of the existing configurations of membrane reactors, development of the catalysts and membrane materials, and published papers in this area was given by Marcano and Tsotsis [1], Julbe et al. [2], Dixon [3], Drioli et al. [4], Dittmeyer [5] and Coronas and Santamaria [6]. In many publications [7–12] the selectivity and the yield of a desired intermediate product B were investigated experimentally in a CMR following the simplified reaction scheme:

$$A + O_2 \rightarrow B,$$

$$B + O_2 \rightarrow C + D,$$

where A is an alkane, C and D are end products (CO_2, H_2O). If the partial pressure of oxygen is of lower order in the desired reaction rate expression than in the expression for the undesired reaction, the oxygen should be fed into the reactor through a membrane. Thereby, better selectivity and yield of the intermediate product are expected in the membrane reactor than in the Packed Bed Reactor (PBR) [13]. However, this advantage of the membrane reactor is linked to a decrease in conversion caused by lower reactant concentrations at the reactor entrance.

Different reactor configurations, like Packed Bed Membrane Reactor (PBMR), Monolith-like Reactor, Catalytic Membrane Reactor (CMR), were investigated and compared by many authors [14–16]. Better selectivities and yields of intermediate products were attained with the membrane reactors than with the traditional PBR.

Akin and Lin [17] reported ethylene yields of 56% and selectivities of 80% for the selective oxidation of ethane to ethylene in a PBMR at 875 °C. Tonkovich et al. [18] also investigated the oxidative dehydrogenation of ethane to ethylene in a tubular PBMR with fixed oxygen dosage through the membrane to establish the influence of the ethane/oxygen ratio, temperature and residence time on the performance of the reactor. Their experimental studies

* Corresponding author. Tel.: +49 391 67 18575; fax: +49 391 67 12762.
E-mail address: Juergen.Schmidt@vst.Uni-Magdeburg.de (J. Schmidt).

0920-5861/$ – see front matter © 2005 Elsevier B.V. All rights reserved.
doi:10.1016/j.cattod.2005.03.081

Nomenclature

a_0	thermal diffusivity (m^2/s)
B	permeability (m^2)
c_i	molar concentration ($kmol/m^3$)
c_p	specific heat capacity (J/(kg K))
C	conversion of ethane $\left(\frac{kg_{ethane,0}-kg_{ethane,z}}{kg_{ethane,0}}\right)$
d_h	hydraulic diameter (m)
D	diffusion coefficient (m^2/s)
$E_{A,j}$	activation energy (j/kmol)
$f_1=\frac{\eta}{B}$	viscous resistance factor (Pa s/m^2)
f_2	inertial resistance factor
$\Delta_R\tilde{h}_j$	enthalpy of reaction j (kJ/kmol)
$\Delta_R h_{1,0}$	dimensionless reaction enthalpy
$I_{v,d}$	momentum source term in direction d (Pa/m)
$k_{\infty,j}$	reaction constant $\left[\frac{kmol^{1-\alpha-\beta}\cdot m^{3(\alpha+\beta)}}{kg\,s\,K^{\alpha+\beta}}\right]$
L	length (m)
$\tilde{M}_i$	molar mass of species i (kg/kmol)
p	pressure (Pa)
$p^*=\frac{p-p_0}{\rho_0 v_{z,0}^2}$	dimensionless pressure
Pr	Prandtl number
$\dot{r}_j$	rate of reaction j ($kmol/m^3$ s)
$\dot{r}_{1,0}$	reaction rate of ethylene formation at T_0 and by $y_{C_2H_6,0}, y_{O_2,0}$ ($kmol/m^3$ s)
Re	Reynolds number
s	height of product channel (m)
S	selectivity of ethylene $\left(\frac{kg_{ethylene,z}}{kg_{ethane,0}-kg_{ethane,z}}\right)$
Sh	Sherwood number
T	temperature (K)
$T^*=\frac{T}{T_0}$	dimensionless temperature
v	velocity (m/s)
$\vec{v}^*=\frac{\vec{v}}{v_{z,0}}$	dimensionless velocity
$y_i=\frac{\rho_i}{\rho}$	mass fraction of species i
y, z	coordinates (m)
$y^*=\frac{y}{d_h}$	dimensionless coordinate
Y	yield of ethylene $\left(\frac{kg_{ethylene,z}}{kg_{ethane,0}}\right)$
$z^*=\frac{z}{d_h}$	dimensionless coordinate

Greek letters

α, β	component order in the reaction
δ	zone thickness (m)
η	dynamic viscosity (kg/(m s))
λ	coefficient of heat conduction (W/(m K))
ν	cinematic viscosity (m^2/s)
$\nu_{i,j}$	stoichiometric coefficient
ρ	density (kg/m^3)

Subscripts and superscripts

0	entrance
C	catalyst
d	coordinate direction
eff	effective
i	component of a reaction
j	number of reactions
mix	mixture
k	zone
M	membrane
St	standard
y, z	coordinates
*	dimensionless variable

confirmed that the membrane reactor outperforms a PBR under low feed ratio conditions.

The performance of membrane reactors depends on the reactor geometry, the membrane structure and the operating conditions. The determination of the optimal conditions demands extensive experiments. Therefore, the simulation approach is favorable for process analysis and parameter optimization [13,19,20]. Most of the authors presented 1D models for the description of catalytic membrane reactors [11,20–22]. In Saracco et al. [23], an isothermal model was developed based on the differential mass balance equations and considering the Dusty Gas Model. This model properly fits the experimental data for high operating temperatures (transport-controlled regime), but it fails to describe the transition from kinetics- to transport-controlled regimes. Thus, a non-isothermal model was developed in later investigations [11].

The application of 2D models has received growing interest in the recent years. This concerns the PBMR [24,25] as well as the CMR [10,26,27]. Marcano and Tsotsis [1] developed a generic model of a Packed Bed Catalytic Membrane Reactor (PBCMR), which takes into account the mass and energy balances, and incorporates the models of Tayakout et al. [27] and Dixon and co-workers [28]. Detailed models were also presented by Brinkmann et al. [10] and Pedernera et al. [26], where both axial and radial concentration profiles in the membrane were taken into account.

In the present work, the application of a CMR to selective partial oxidation of ethane is investigated using the software package FLUENT®. The transport processes and chemical reactions are described in detail by a two-dimensional steady-state model. The simulations serve as a basis for the analysis and evaluation of the influence of the reactor's operating conditions and geometrical parameters on the yield of ethylene. This study aims to provide a better understanding of the sub-processes, especially the transport phenomena in all reactor zones as well as to select effective operating conditions and thereby to reduce the experimental costs.

2. Analyzed reactor configurations

The CMR is described by a three-zone model consisting of product channel, catalyst layer and membrane (Fig. 1).

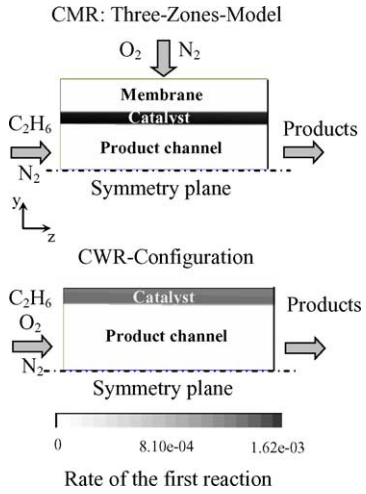

Fig. 1. CMR and CWR configurations and rate of formation of ethylene for a reference case.

The CWR is sketched below and consists of two zones. In both reactor configurations, the product channel and the catalyst layer are identical. The rate of formation of ethylene in the catalyst layer of both reactors for comparable operating conditions is presented as an example.

Both reactors were compared under the conditions that the Reynolds numbers at the inlet of the CWR and at the outlet of the CMR are equal, and that the mass flow of educts is the same. The residence time in the CMR is influenced by the stream across the membrane.

3. Mathematical model

The mathematical model was applied to the partial oxidation of ethane based on a simplified reaction network (cf. Table 1) involving five consecutive and parallel reactions. The following model assumptions were made:

- 2D formulation for plane channels;
- steady-state process;
- Laminar flow conditions due to the small hydraulic channel diameters;
- plug flow at the entrance of the product channel;
- convective transport in the membrane and in the catalyst only in y direction;
- chemical reactions only in the catalyst layer;
- effective transport coefficients in the catalyst layer and in the membrane;
- negligible energy transfer by radiation;
- negligible molecular enthalpy transport of the diffusion stream as well as negligible dissipation term.

By the multi-dimensional modeling the heat and mass transfer are an integral part of the model and there is no need of external formulas for the determination of the heat and mass transfer coefficients.

3.1. Governing equations

The system of differential equations in dimensionless form includes Navier–Stokes and energy transport equations, components and total mass balances.

Navier–Stokes equations

$$\frac{\rho}{\rho_0}\left(v_y^*\frac{\partial v_y^*}{\partial y^*}+v_z^*\frac{\partial v_y^*}{\partial z^*}\right)=-\frac{\partial p^*}{\partial y^*}+\frac{1}{Re}\left(\frac{\partial}{\partial y^*}\frac{\eta}{\eta_0}\left(\frac{4}{3}\frac{\partial v_y^*}{\partial y^*}-\frac{2}{3}\frac{\partial v_z^*}{\partial z^*}\right)+\frac{\partial}{\partial z^*}\frac{\eta}{\eta_0}\left(\frac{\partial v_y^*}{\partial z^*}+\frac{\partial v_z^*}{\partial y^*}\right)\right)-\frac{d_h}{\rho_0}I_{v,y} \tag{1}$$

$$\frac{\rho}{\rho_0}\left(v_y^*\frac{\partial v_z^*}{\partial y^*}+v_z\frac{\partial v_z^*}{\partial z^*}\right)=-\frac{\partial p^*}{\partial z^*}+\frac{1}{Re}\left(\frac{\partial}{\partial y^*}\frac{\eta}{\eta_0}\left(\frac{\partial v_z^*}{\partial y^*}+\frac{\partial v_y^*}{\partial z^*}\right)+\frac{\partial}{\partial z^*}\frac{\eta}{\eta_0}\left(\frac{4}{3}\frac{\partial v_z^*}{\partial z^*}-\frac{2}{3}\frac{\partial v_y^*}{\partial y^*}\right)\right)-\frac{d_h}{\rho_0}I_{v,z} \tag{2}$$

Momentum source term for homogenous porous media

$$I_{v,d}=f_1 v_d^*+f_2|v_d^*|v_d^*,\quad f_2=0 \tag{3}$$

Continuity equation

$$\frac{\partial(\rho v_y^*)}{\partial y^*}+\frac{\partial(\rho v_z^*)}{\partial z^*}=0 \tag{4}$$

Transport equations for species

$$\frac{\rho}{\rho_0}\left(v_y^*\frac{\partial y_i}{\partial y^*}+v_z^*\frac{\partial y_i}{\partial z^*}\right)=\frac{1}{Re\,Sc}\left(\frac{\partial}{\partial y^*}\frac{\rho}{\rho_0}\frac{D_{i,\mathrm{mix}}}{D_0}\frac{\partial y_i}{\partial y^*}+\frac{\partial}{\partial z^*}\frac{\rho}{\rho_0}\frac{D_{i,\mathrm{mix}}}{D_0}\frac{\partial y_i}{\partial z^*}\right)+\sum_j Da\nu_{ij}\frac{\tilde{M}_i}{\tilde{M}_{C_2H_4}}\frac{\dot{r}_j}{\dot{r}_{1,0}} \tag{5}$$

Energy equation

$$\frac{\rho c_p}{(\rho c_p)_0}\left(v_y^*\frac{\partial T^*}{\partial y^*}+v_z^*\frac{\partial T^*}{\partial z^*}\right)=\frac{1}{Re\,Pr}\left(\frac{\partial}{\partial y^*}\frac{\lambda}{\lambda_0}\frac{\partial T^*}{\partial y^*}+\frac{\partial}{\partial z^*}\frac{\lambda}{\lambda_0}\frac{\partial T^*}{\partial z^*}\right)+\sum_j Da\frac{\Delta_R\tilde{h}_{1,0}}{M_{C_2H_4}c_{p,0}T_0}\frac{\Delta_R\tilde{h}_j}{\Delta_R\tilde{h}_{1,0}}\frac{\dot{r}_j}{\dot{r}_{1,0}} \tag{6}$$

All geometrical dimensions were related to the hydraulic diameter of the product channel $d_h = 2$ s. The use of dimensionless parameters allows for the applicability of the results to all similar cases.

Table 2 shows the influencing dimensionless groups. Among these are counted the geometrical ratios, like the ratio of catalyst or membrane thickness to hydraulic diameter and the operating parameters, like mass fraction of oxygen $y_{O_2,0}$ and velocity ratio $v_y^* = v^* = v_M/v_{z,0}$.

Table 1
Reaction kinetics

No.	Reaction	$\Delta_R\tilde{h}_j$ by ρ_{St}, ϑ_{St} (kJ/kmol)	$k_{\infty,j}$ ($\frac{kmol^{1-\alpha-\beta}\,m^{3(\alpha+\beta)}}{kg\,s\,K^{\alpha+\beta}}$)	$E_{A,j}$ (J/kmol)	α_j	β_j
1	$C_2H_6 + 0.5O_2 \rightarrow C_2H_4 + H_2O$	105040	0.488	82.9e + 6	0.88	0.06
2	$C_2H_6 + 3.5O_2 \rightarrow 2CO_2 + 3H_2O$	1427780	15.19	114.6e + 6	0.75	0.30
3	$C_2H_4 + 2O_2 \rightarrow 2CO + 2H_2O$	756800	2.07e − 3	40.9e + 6	0.84	0.11
4	$C_2H_4 + 3O_2 \rightarrow 2CO_2 + 2H_2O$	1322740	1.79e − 3	58.4e + 6	0.87	0.20
5	$CO + 0.5O_2 \rightarrow CO_2$	282970	3.58e − 4	32.2e + 6	1.12	0.12

The momentum source term, which can be formulated in equation (3) by using experimentally determined coefficients f_1 and f_2, was considered in the membrane and in the catalyst layer. A linear equation was chosen as simplification for small velocities. The calculation of the velocity fields in the membrane and in the catalyst was based on the conditions of fully developed flow ($v_y = f(z)$, $\partial v_y/\partial y = 0$, $v_z = 0$, $\partial p/\partial y = \text{const}$). At appropriate values of f_1 the membrane and the catalyst layer were flown through with a locally constant velocity $v_{y,M}$, which dropped to the value $v_y = 0$ in thin layers at both reactor inlet ($z = 0$) and outlet ($z = 1$). Thereby, compliant numerical conditions resulted at the crucial vertices of reactor's entrance and exit.

The reaction source terms in the energy and mass balances were taken into account only in the thin catalyst layer of thickness δ_C. The mass balances (5) were solved for the six species: oxygen, ethane, ethylene, carbon monoxide, carbon dioxide and water. The concentration of the inert component (nitrogen) is calculated from the relation $\Sigma y_i = 1$. The diffusion streams are related to the mean velocity of the center of gravity.

The governing equations were solved under the following boundary conditions: plug flow in the product channel ($v^*_{z,0} = 1$) and along the membrane ($v^* = \text{const}$), constant inlet temperature $T^* = 1$ for both membrane and product channel and constant inlet mass fractions of ethane $y_{C_2H_6,0}$ and oxygen $y_{O_2,0}$. The flow through the membrane corresponds to a determined pressure distribution in the O_2-channel, which depends on the properties of the membrane.

3.2. Physical properties and reaction kinetics

The gas phase is considered as a mixture of ideal gases. Because of the low concentration of reactants, the physical properties of nitrogen were applied to approximate the behavior of the mixture. Specific heat capacity c_p, viscosity η and thermal conductivity λ at the operating temperature were calculated according to Krauss and Span [29]. A simplified treatment of diffusive mass transport is possible by using binary diffusion coefficients for each species in the mixture (mix), respectively, in the inert excess species. The required binary diffusion coefficients $D_{i,mix}$ at the operating temperature were calculated by the method of Fuller, Schettler and Giddings [29].

Table 2
Influencing dimensionless groups

$Re = \frac{v_{z,0} d_h \rho}{\eta_0}$	$Da = \frac{\tilde{M}_{C_2H} d_h \rho_C \dot{r}_{1,0}}{\rho_0 v_{z,0}}$
$v^*_y = \frac{v_M}{v_{z,0}}$	$\Delta_R h_{1,0} = \frac{\Delta_R \tilde{h}_{1,0}}{\tilde{M}_{C_2H_4} c_{p,0} T_0}$
$Pr = \nu_0/a_0$,	$y_{C_2H_6,0}, y_{O_2,0}$
$Sc = \nu_0/D_0$	$\frac{\eta_{eff,k}}{\eta_0}, \frac{\lambda_{eff,k}}{\lambda_0}, \frac{D_{eff,k}}{D_0}$
δ_M/d_h	δ_C/d_h

The transport processes in the membrane and in the catalyst layer were formulated under the assumption of porous layers with effective transport coefficients η_{eff}, λ_{eff} and D_{eff}. These can depend on the location, especially in the case of a multilayer configuration. The effective thermal conductivities of the membrane and the catalyst layer were approximated by using the values of the solid and gas phase considering the porosity according to [29] and assumed to be constant. The effective diffusion coefficients for each species were estimated following the Bosanquet scheme [30] by means of a series of diffusion resistances, i.e. as a function of the molecular and Knudsen diffusivities.

The required material parameters are given in Table 3.

The applied reaction kinetics was determined experimentally [31] for catalyst particles with 1.8 mm diameter and described by power law equations. The reaction kinetics was assumed to be valid for a catalyst layer with plane geometry. The equation form (7) and the values in Table 1 were used for the numerical simulations.

$$r_j = \rho_C T^{\alpha_j+\beta_j} k_{\infty,j} \exp\left(-\frac{E_{A,j}}{\tilde{R}T}\right) c_{C_j}^{\alpha_j} c_{O_2}^{\beta_j} \tag{7}$$

The temperature factor $T^{\alpha+\beta}$ enables an easy conversion to other temperature dependent variables of composition. The experimentally determined reaction rates were referred to the inserted mass of the catalyst [31]. The factor ρ_C serves to convert the reaction rate per catalyst volume because a pseudo-homogenous approach is used for the catalyst layer.

3.3. Method of solution

The CFD program FLUENT® was used for the numerical solution. It is based on the finite volume method. FLUENT® incorporates an effective equation solver with user-friendly modules for pre- and post-processing. The modeling of the complex conditions of the membrane reactor requires user-defined functions. Preparatory tests were performed for

Table 3
Operating conditions for the CMR

Product channel	Membrane and catalyst layer
$\rho_{N_2} = 0.39$ kg/m^3	$\rho_C = 1020$ kg/m^3
$\eta_{N_2} = 3.8 \times 10^{-5}$ Pa s	$\eta_{N_2} = 3.8 \times 10^{-5}$ Pa s
$c_p = 1140$ J/kg K	$c_p = 1140$ J/kg K
$\lambda_{N_2} = 0.005816$ W/m K	$\lambda_{eff} = 0.4$ W/m K
$T_0 = 863.15$ K	$T_0 = 863.15$ K
$D_{i,N_2} \sim 10^{-4}$ m^2/s	$f_1 = 10 \times 10^7$ Pa s/m^2
$p = 0.1$ MPa	$f_2 = 0$
	$D_{i,N_2} \sim 10^{-6}$ m^2/s

some problems with known analytical solutions. The results were compared for thermally and hydrodynamically developing flows in pipes and channels [32]. In addition, the velocity fields of a packed bed reactor were calculated. The numerical results were in good agreement with the analytical solution in all simulation cases. Subsequently, the grid independence of the solution was verified for the membrane reactor. The results showed that 80 cells in both coordinate directions already provided a sufficient accuracy. The number of cells in y direction was 40 for the product channel and 20 for the catalyst layer as well as for the membrane. For all calculations the accuracy of the energy balance and of the mass balances was controlled along the reactor.

4. Simulation results and discussion

A reference case was defined as basis for the parameter variation. Fig. 2 and Table 3 show the reactor geometry and the operating parameters. The velocity v_M is kept constant along the reactor. The composition of the reactants, the membrane and the catalyst layer properties were chosen according to the conditions of accomplished experiments in the research group and to the area of validity of the reaction kinetics [31,33,34]. The maximum values of concentrations and temperatures at the explosion limits were taken into account.

The selectivity and the conversion were calculated on the basis of mass streams. The yield is defined as the product of conversion and selectivity.

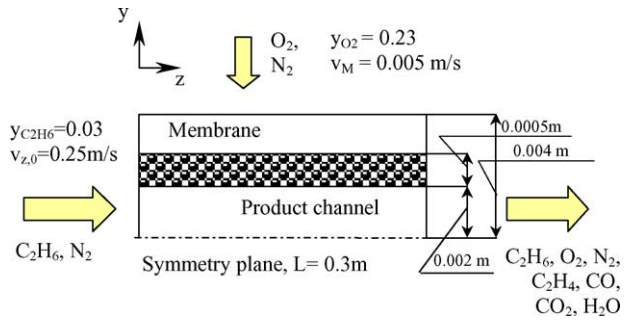

Fig. 2. Operating conditions for the CMR.

The simulations served to analyze the influence of the following parameters on the yield of ethylene:

$y_{O_2,M}$	oxygen fraction in membrane stream
$v^* = v_M/v_{z,0}$	velocity ratio
Re	in reference to product channel inlet
$y_{C_2H_{6,0}}$	ethane fraction at product channel inlet
T/T_0	influence of the temperature
δ_C/d_h	influence of catalyst layer thickness

The increase of the temperature in the CMR is small under the given conditions. Therefore, most of the calculations were performed without considering the energy balance.

Fig. 3 shows the distribution of ethane in the reactor for the reference case. The mass diffusion of ethane is influenced by the convective flux and the higher diffusion resistance in the membrane. In the catalyst layer and in the product channel the mass fraction decreases along the reactor because of reactions and permanent dilution. The ethane gradients become zero inside the membrane. At this stage, it is important to clarify that ethane is transported towards the catalyst layer only by diffusion. The convective fluxes through the membrane and the higher diffusion resistances act in the opposite direction. Hence, the velocity through the membrane in the CMR should be lower than the velocity in the PBMR. This phenomenon brings up another problem of the catalytic membrane reactor namely to avoid loss of reactants by diffusion through the membrane. There are several possibilities:

- increase of the trans-membrane stream;
- enlargement of the membrane layer thickness;
- application of membrane layers with smaller mean pore diameter and higher diffusion resistances.

From this follows an optimization problem of CMR: due to the increase of the trans-membrane stream, less ethane reaches the catalyst layer. Thus, less ethylene is generated. Thicker membranes cause higher-pressure drops of the membrane stream.

Fig. 4 shows the distribution of ethylene in the reactor for the reference case. Near the inlet, the ethylene mass fraction

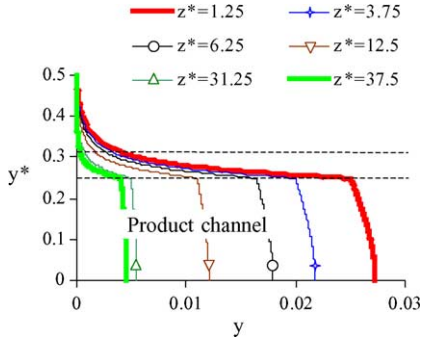

Fig. 3. Mass fraction of ethane in the reactor.

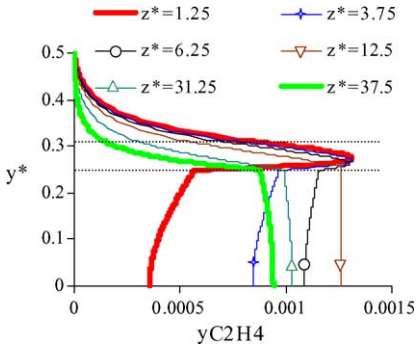

Fig. 4. Mass fraction of ethylene in the reactor.

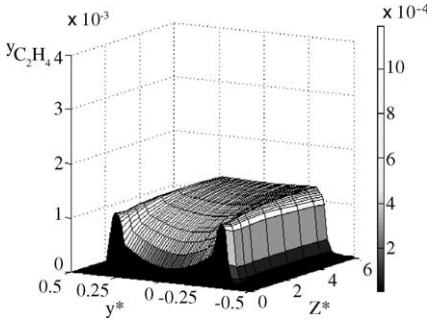

Fig. 6. Mass fraction of ethylene in the reactor for a high trans-membrane stream.

increases rapidly, particularly in the catalyst layer, and consequently it rises also in the product channel. Ethylene is an intermediate product and after a certain reactor length its consumption is higher than its production, i.e. the mass fraction begins to decrease.

The next figures (Figs. 5 and 6) present the influence of the flux through the membrane on the ethylene profiles. The decrease of the mass fraction of ethylene is caused by the suppressed diffusion of ethane to the catalyst layer due to higher flow rate through the membrane. The influence of the flux through the membrane on the rate of the desired reaction is shown in Figs. 7 and 8. The higher side streams decrease the reaction rate significantly and only a thin layer of the catalyst is active.

In the following investigations, the reference case was taken as a basis for the variation of the parameters. Only the influence of one parameter on the yield and the selectivity of ethylene was investigated in each case.

4.1. Influence of oxygen dosage

The oxygen mass fraction was varied within the range $0.001 < y_{O_2} < 0.23$. Fig. 9 shows that a decrease of the oxygen amount causes an increase of the ethylene yield. In the case of $y_{O_2} = 0.005$, the maximum ethylene yield is achieved. A further lowering of y_{O_2} down to 0.001 significantly decreases the conversion and the yield.

By increasing the trans-membrane stream the oxygen amount becomes larger in the catalyst layer and less ethane reaches the catalyst since higher membrane flow rates constrain the ethane diffusion. Hence, the yield of ethylene decreases with increasing flow rate through the membrane.

4.2. Influence of Reynolds number and ethane mass fraction

Fig. 10 shows the strong influence of the Reynolds number and thus of the residence time on the yield of ethylene. In the reference case, the Reynolds number at the inlet is 20. Low values of the Reynolds number cause an increase of the conversion of ethane and a decrease in the selectivity to ethylene. By decreasing the Reynolds number the maximum of the yield curve is shifted to shorter reactor lengths.

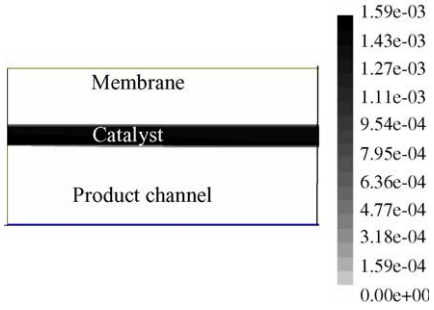

Fig. 7. Rate of formation of ethylene for a low trans-membrane stream.

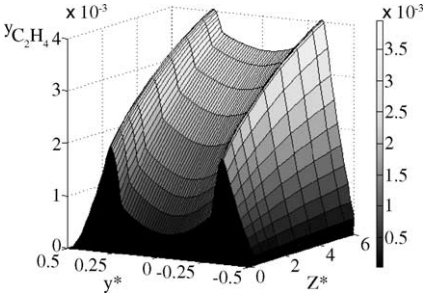

Fig. 5. Mass fraction of ethylene in the reactor for a low trans-membrane stream.

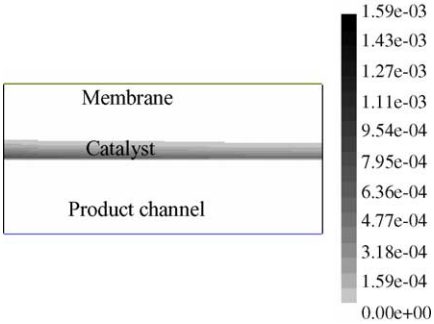

Fig. 8. Rate of formation of ethylene for a high trans-membrane stream.

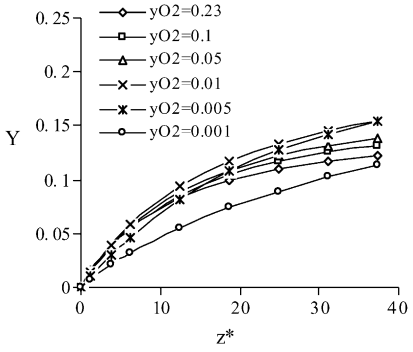

Fig. 9. Influence of the mass fraction of oxygen on the yield of ethylene.

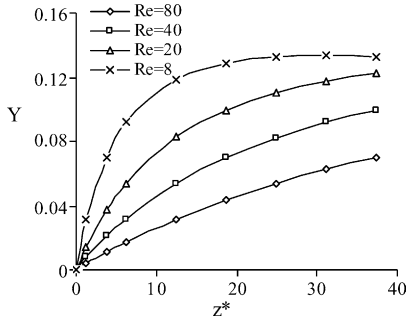

Fig. 10. Influence of the Reynolds number on the yield of ethylene.

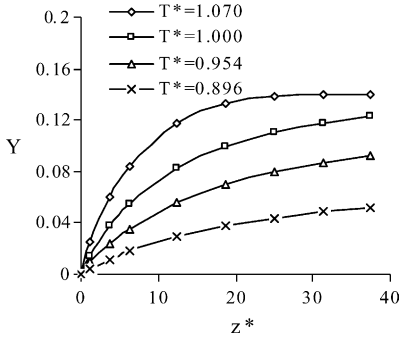

Fig. 12. Influence of the temperature on the yield of ethylene.

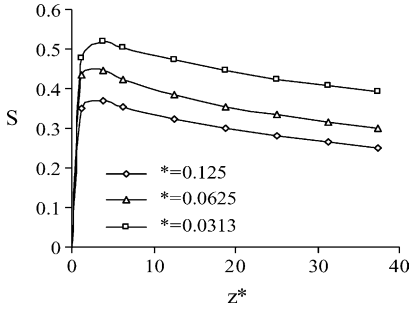

Fig. 13. Influence of the catalyst layer thickness δ^* on the selectivity of ethylene.

The influence of the ethane mass fraction is rather small in the range $0.005 < y_{C_2H_6} < 0.05$. A maximum yield is obtained for $y_{C_2H_6} = 0.05$. High values of the ethane mass fraction improve the selectivity and the yield of ethylene.

4.3. Influence of temperature

Simulations for different temperatures were performed under isothermal conditions. In spite of the higher selectivity at low temperature, the highest yield of ethylene was obtained at the highest temperature because of the increased conversion (Figs. 11 and 12).

4.4. Influence of catalyst layer thickness

Simulations were accomplished for the reference case using different catalyst layer thicknesses ($0.0313 < \delta_C/d_h < 0.125$). As expected, the highest selectivity is obtained under the given conditions in the case with the thinnest catalyst layer (Fig. 13). At the reactor outlet, the ethylene yield for the catalyst layer thickness $\delta^* = 0.0625$ is still higher than the yield for the thinnest catalyst layer (Fig. 14), although the tendency can be clearly recognized; the decrease of the catalyst layer thickness results in an enhancement of the selectivity and the yield of the desired intermediate product. A thicker catalyst layer improves the conversion of ethane, but the selectivity has the dominant influence on the yield.

4.5. CMR in comparison with CWR

The simulations for the CWR were performed only for comparison. In relation to the commonly used PBR, a CWR

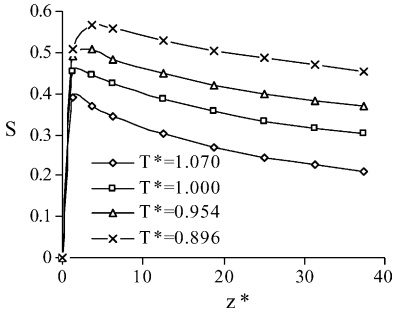

Fig. 11. Influence of the temperature on the selectivity of ethylene.

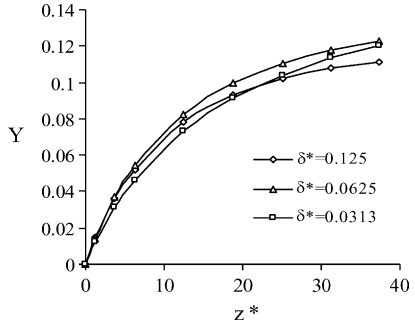

Fig. 14. Influence of the catalyst layer thickness δ^* on the yield of ethylene.

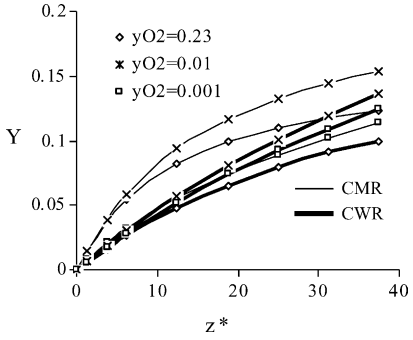

Fig. 15. Influence of y_{O_2} on the yield curves in CMR and CWR.

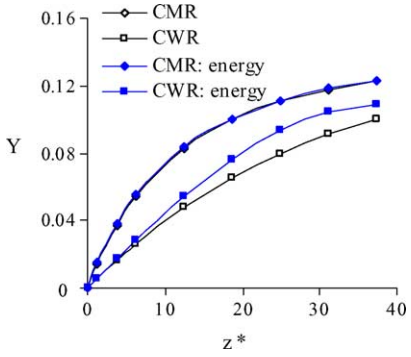

Fig. 16. Temperature influence on the yield of ethylene in CMR and CWR.

can be of interest in the case of small characteristic lengths, a condition encountered for example in monolith reactors. The reference case was again the basis for the simulation. The total membrane stream of the CMR was fed at the inlet of the CWR and hence the residence times are shorter. The corresponding oxygen mass fraction is smaller because of the higher inlet mass flow rate.

The simulation results (Figs. 15 and 16) show clearly the following advantages of the CMR in comparison to the CWR:

- The obtained ethylene yield in the CMR is higher than the yield in the CWR for shorter reactor lengths.
- The CMR offers a better temperature control for highly exothermic serial–parallel reactions.

To evaluate the potential of both reactors, it is necessary to perform a comparison under the optimal conditions for each reactor.

5. Conclusions

From the simulations performed in this work the following conclusions can be drawn:

- Heterogeneous models and multidimensional formulation are necessary for the complete description of a CMR.
- The oxygen dosage affects significantly selectivity and yield of ethylene:
  - Lower flow rate through the membrane is necessary in the CMR in comparison to the PBMR. For given membrane properties the convective stream through the membrane influences strongly the activity of the catalyst layer and the effectiveness of the reactor.
  - The yield of ethylene increases with decreasing oxygen mass fraction until to a determined value. Further reduction of the oxygen mass fraction affects strongly the conversion and lowers the yield.
- $v_M/v_{z,0}$, $\delta_C/D_{\text{eff},k}$, $\delta_M/D_{\text{eff},M}$ influence strongly:
  - the activity of the catalyst layer and
  - the transfer of products to the oxygen channel.
- The dosage of oxygen through the membrane enables the operation of the reactor over a wide range of parameters. This clarifies the advantages of a CMR in comparison to a PBMR. The porosity distribution in a PBMR can cause hot spots and undesirable reactor behavior.
- The results of the different simulations show clearly the advantages of the CMR compared to the CWR.

Further systematic simulations are necessary to determine the effective operating conditions for defined membrane configurations. Hence, model improvements and adjustments to the experimental results, concerning the reaction kinetics and membrane properties, are necessary.

Acknowledgement

The financial support of the German Research Foundation (research group ‘‘Membrane supported reaction engineering’’, FOR 447/1-1) is gratefully acknowledged.

References

[1] J.G.S. Marcano, T.T. Tsotsis, Catalytic Membranes and Membrane Reactors, Wiley-VCH Verlag GmbH, Weinheim, 2002.
[2] A. Julbe, D. Farrusseng, Ch. Guizard, J. Membr. Sci. 181 (2001) 3–20.
[3] A. Dixon, Int. J. Chem. Reactor Eng. 1 (2003) R6 http://www.bepress.com/ijcre/vol1/R6/.
[4] E. Drioli, A. Criscuoli, E. Curcio, Chem. Eng. Technol. 26 (9) (2003) 975–981.
[5] R. Dittmeyer, in: Proceedings of the DGMK-Conference ‘‘Chances for Innovative Processes at the Interface Between Refining and Petrochemistry’’, October 2002, Berlin, pp. 131–145.
[6] J. Coronas, J. Santamaria, Catal. Today 51 (1999) 277–389.
[7] A. Bottino, G. Capannelli, A. Comite, J. Membr. Sci. 197 (1–2) (2002) 75–88.
[8] M.J. Alfonso, A. Julbe, D. Farrusseng, M. Menéndez, J. Santamaría, Chem. Eng. Sci. 54 (1999) 1265–1272.
[9] M.J. Alfonso, M. Menéndez, J. Santamaría, Catal. Today 56 (1–3) (2000) 247–252.
[10] T. Brinkmann, S.P. Perera, W.J. Thomas, Chem. Eng. Sci. 57 (2002) 2531–2544.
[11] G. Saracco, V. Specchia, Chem. Eng. Sci. 55 (2000) 3979–3989.
[12] H.W.J.P. Neomagus, G. Saracco, H.F.W. Wessel, G.F. Versteeg, Chem. Eng. J. 77 (2000) 165–177.
[13] A. Dixon, Catal. Today 67 (2001) 189–203.

[14] G. Capannelli, E. Carosini, F. Cavani, O. Ponticelli, F. Trifiro, Chem. Eng. Sci. 51 (1996) 1817–1826.
[15] L. Paturzo, F. Gallucci, A. Basile, G. Vitulli, P. Pertici, Catal. Today 82 (2003) 57–65.
[16] F. Klose, T. Wolff, S. Thomas, A. Seidel-Morgenstern, Catal. Today 82 (2003) 25–40.
[17] F.T. Akin, Y.S. Lin, J. Membr. Sci. 209 (2) (2002) 457–467.
[18] A. Tonkovich, J. Zilka, D. Jimenez, G. Roberts, J. Cox, Chem. Eng. Sci. 51 (1996) 789–806.
[19] V. Diakov, A. Varma, Ind. Eng. Chem. Res. 43 (2) (2004) 309–314.
[20] L. Li, R. Borry, E. Iglesia, Chem. Eng. Sci. 57 (2002) 4595–4604.
[21] J. Sousa, P. Cruz, A. Mendes, J. Membr. Sci. 181 (2001) 241–252.
[22] A. Yawalkar, V. Pangarkar, G. Baron, J. Membr. Sci. 182 (2001) 129–137.
[23] G. Saracco, J. Veldsink, G. Versteeg, W. van Swaaij, Chem. Eng. Sci. 50 (1995) 2833–2841.
[24] K. Hou, R. Hughes, R. Ramos, M. Menéndez, J. Santamaria, Chem. Eng. Sci. 56 (2001) 57–67.
[25] S. Assabumrungrat, T. Rienchalanusarn, P. Praserthdam, S. Goto, Chem. Eng. J. 85 (2002) 69–79.
[26] M. Pedernera, M.J. Alfonso, M. Menendez, J. Santamaria, Chem. Eng. Sci. 57 (13) (2002) 2531–2544.
[27] M. Tayakout, B. Bernauer, Y. Toure, J. Sanchez, Simul. Practice Theor. 2 (1995) 205–219.
[28] Y. Becker, A. Dixon, W. Moser, Y. Ma, J. Membr. Sci. 77 (1993) 197.
[29] VDI-Wärmeatlas, 9, Auflage, Springer, 2002, Chapters Da, Db and Dee.
[30] N. Wakao, J.M. Smith, Chem. Eng. Sci. 17 (1962) 825–834.
[31] F. Klose, M. Joshi, C. Hamel, A. Seidel-Morgenstern, Appl. Catal. A: Gen. 260 (1) (2004) 101–110.
[32] D. Handtke, I. Mednev, J. Schmidt, in: Proceedings of the Fourth European Thermal Sciences Conference, Paper No. POM 8, Birmingham, UK, March, 2004.
[33] A. Hussain, E. Tsotsas, Wärme- und Stofftransport in anorganischen, rohrförmigen Membranen, GVC-Fachausschuß ''Wärme- und Stoffübertragung'', Schwäbisch Hall, March, 2004.
[34] A. Hussain, S. Silalahi, E. Tsotsas, in: Proceedings of the Fourth European Thermal Sciences Conference, Paper No. POM 5, Birmingham, UK, March, 2004.